Journal for ImmunoTherapy of Cancer

Single-cell spatial transcriptomics unravels cell states and ecosystems associated with clinical response to immunotherapy

Ziena Abdulrahman ,[1,2] Roderick C Slieker,[1,3] Daniel McGuire,[4] Marij J P Welters,[1,2] Mariette I E van Poelgeest,[5] Sjoerd H van der Burg [1,2]

To cite: Abdulrahman Z, Slieker RC, McGuire D, *et al*. Single-cell spatial transcriptomics unravels cell states and ecosystems associated with clinical response to immunotherapy. *Journal for ImmunoTherapy of Cancer* 2025;**13**:e011308. doi:10.1136/jitc-2024-011308

► Additional supplemental material is published online only. To view, please visit the journal online (https://doi.org/10.1136/jitc-2024-011308).

Accepted 25 February 2025

[1]Department of Medical Oncology, Leiden University Medical Center, Leiden, ZH, Netherlands
[2]Oncode Institute, Utrecht, Netherlands
[3]Department of Cell and Chemical Biology, Leiden University Medical Center, Leiden, Netherlands
[4]NanoString Technologies Inc, Seattle, Washington, USA
[5]Gynaecology, Leiden University Medical Center, Leiden, Zuid-Holland, Netherlands

Correspondence to
Dr Sjoerd H van der Burg; shvdburg@lumc.nl

ABSTRACT

Background The tumor microenvironment (TME) is a complex and dynamic ecosystem that is known to influence responses to immunotherapy. We leveraged single-cell spatial transcriptomics to systematically dissect the intricate complexity of the TME, in particular the cellular heterogeneity and spatial interactions. Their collective impact on immunotherapy efficacy was studied in the context of a homogeneous group of patients with vulvar high-grade squamous intraepithelial lesions (vHSIL) treated with an immunotherapeutic tumor-specific peptide vaccine.

Methods We performed single-cell spatial transcriptomics on 20 pretreatment vHSIL lesions, stratified by clinical response to immunotherapeutic vaccination into complete responders (CR), partial responders (PR) and non-responders (NR). Using a 1,000-gene panel, we mapped over 274,000 single cells in situ, identifying 18 cell clusters and 99 distinct non-epithelial cell states. Findings were validated against public single-cell transcriptomic data sets to assess their broader relevance across tumor types.

Results Profound heterogeneity within the TME was detected across the response groups. CR lesions exhibited a higher ratio of immune-supportive to immune-suppressive cells—a pattern mirrored in other solid tumors following neoadjuvant checkpoint blockade. Key immune populations enriched in CRs included CD4+CD161+ effector T cells and chemotactic CD4+ and CD8+ T cells. Conversely, PRs were characterized by increased proportions of T helper 2 cells and CCL18-expressing macrophages, which are associated with the recruitment of type 2 T cells and regulatory T cells. NRs displayed preferential infiltration with immunosuppressive fibroblasts. Distinct spatial immune ecosystems further defined response groups. Although a number of immune cells were detected in all patients, type 1 effector cells dominated interactions in CRs, type 2 cells were prominently interacting in PRs, while NRs lacked organized immune cell interactions.

Conclusions This study underscores the dual importance of both cellular composition and spatial organization in steering clinical response to immunotherapy.

WHAT IS ALREADY KNOWN ON THIS TOPIC

⇒ The tumor microenvironment (TME) plays a critical role in determining responses to immunotherapy. Studies focused on predefined cell populations have identified several cells associated with treatment outcomes but simultaneously underscored the difficulty of using them as reliable biomarkers.

WHAT THIS STUDY ADDS

⇒ This study confirms the significant heterogeneity in the cellular composition of vulvar high-grade squamous intraepithelial lesions and demonstrates that in particular the differences in spatial organization of immune cell states are associated with clinical response to immunotherapy.

HOW THIS STUDY MIGHT AFFECT RESEARCH, PRACTICE OR POLICY

⇒ These findings underscore the importance of spatially resolved single-cell analyses in understanding the TME and suggest that targeting immune-supportive ecosystems could optimize immunotherapeutic strategies across tumor types.

INTRODUCTION

Over the past decade, there has been a significant surge in T cell-based immunotherapeutic approaches for cancer treatment, including immune checkpoint blockade, adoptive cell therapy, and therapeutic vaccines.[1–3] While these strategies have achieved remarkable success, many patients either fail to respond or experience only transient benefits. This underscores a critical need to deepen our understanding of how patient-specific tumor characteristics influence therapeutic responses. Retrospective analyses, typically focused on predefined markers and cell populations, have identified several tumor microenvironment (TME) features associated with treatment outcomes.[4 5] However, the intricate complexity of the TME, particularly the cellular heterogeneity and spatial

interactions, remains insufficiently understood, as does their collective influence on immunotherapy efficacy. Deciphering the multifaceted ecosystem of the TME—comprising diverse tumor, immune, and stromal cell populations, their cellular states, and their spatial interactions—could provide valuable insights into its role in modulating responses to specific immunotherapeutic interventions.[6–9] Such an understanding has the potential to guide the identification of novel therapeutic targets and optimize patient selection, thereby enhancing the efficacy of immunotherapy.

In two clinical trials, we observed complete regression or partial regression in approximately half of the patients with human papillomavirus type 16 (HPV16)-induced vulvar high-grade squamous intraepithelial lesions (vHSIL) following treatment with an immunotherapeutic tumor-specific peptide vaccine comprising HPV16 E6/E7-specific synthetic long peptides.[10 11] Importantly, vHSIL patients represent a relatively homogeneous cohort, devoid of confounding factors such as differences in gender,[12] stage, oncogenic pathways,[13–15] or tumor location.[16] These factors, known to influence TME composition, often complicate studies investigating the relationship between the TME and treatment outcomes. Clinical responsiveness in these trials correlated with the magnitude of the vaccine-induced systemic T-cell response[11 17] and with a pre-existing abundance of T cells and myeloid cells within the TME prior to vaccination.[18] This association highlights the importance of the baseline immune landscape in determining therapeutic success and provides a foundation for further exploration of how TME features shape immunotherapy outcomes.

In this study, we employed single-cell spatial transcriptomics to measure RNA expression at subcellular resolution in formalin-fixed, paraffin-embedded (FFPE) whole tissue samples.[19] This approach combines the high-resolution analytical power of single-cell RNA sequencing with the spatial context provided by in situ imaging. Consequently, it enables the interrogation of cellular heterogeneity without relying on predefined marker sets,[9 20–23] allowing for a comprehensive digital reconstruction of the cellular landscape within these lesions. Furthermore, this methodology facilitated an in-depth analysis of cellular states and spatial interactions within TME in relation to clinical responses to immunotherapy. Key findings from this analysis were validated using publicly available immunotherapy data sets, underscoring the robustness and translational relevance of the results.

MATERIALS AND METHODS

Patient samples

Pre-vaccination FFPE biopsies of 20 women of ≥18 years old with histologically confirmed HPV16$^+$ vHSIL were analyzed. These women participated in a phase I/II therapeutic HPV16 SLP vaccination trial with ISA101.[10 11] The ISA101 vaccine was injected subcutaneously and consisted of 13 synthetic long overlapping peptides covering the entire amino acid sequence of HPV16 oncoproteins E6 and E7, emulsified with Montanide adjuvant. Clinical efficacy assessments in the trial were performed 3 and 12 months after the last vaccination. The patients were classified based on their best clinical response 12 months after vaccination without additional treatment into: complete responders (CR, n=6) when the lesion completely disappeared, partial responders (PR, n=7) when ≥50% of the total lesion area had disappeared, and non-responders (NR, n=7) when <50% of the lesion had disappeared. All patients gave written informed consent to participate in this immunotherapeutic trial.

Statistical analyses

Statistical data analyses were performed with GraphPad Prism V.9.3.1 and with R V.4.4.0, which were also used to create graphs to visualize the data. In R, *ggplot2* (V.3.5.1) was used to produce plots. The median immune counts of the three different response groups were compared using the non-parametric Kruskal-Wallis test and of two response groups by the non-parametric Mann-Whitney U test. Bonferroni-corrected p values were marked as statistically significant.

Single-cell spatial transcriptomics

The patient samples, all diagnosed with vHSIL by a specialized pathologist, were analyzed with the CosMx Spatial Molecular Imager (NanoString), which allowed the visualization of 1,000 RNA transcripts at a subcellular resolution in situ on FFPE pre-immunotherapy vHSIL tissue, using cyclic fluorescent in situ hybridization.[19] This technique allowed both the discovery of new cell types in the TME of vHSIL, as well as the exploration of their spatial interactions. The majority of the patients' vHSIL biopsies could be completely covered with fields of view for spatial transcriptomic analysis. Cell segmentation was performed with CellPose, which has been shown to be one of the most reliable methods.[24]

Semi-supervised cell type classification

Cell type classification was performed using the semi-supervised cell typing method InSituType.[25] An initial round of cell typing was run using an immuno-oncology-based cell type reference profile provided as the default in the R software package and allowing for six unsupervised clusters to characterize epithelial cell types. Subsequently, cells which were classified as an immune cell type were further refined by clustering smoothed averages of marker genes for the cell's nearest neighbors (https://nanostring-biostats.github.io/CosMx-Analysis-Scratch-Space/posts/marker-gene-smoothing/). Specifically, a set of 58 genes with known expression specificity in immune cells was pre-selected (online supplemental table 1).

Let $\boldsymbol{X}_{markers\times cells}$ denote a total-count normalized expression matrix for cells classified as non-epithelial and their expression in the pre-selected marker gene set. Let $\boldsymbol{W}_{cells\times cells}$ denote a nearest neighbors matrix where each column indicates the nearest 50 neighbors of the

corresponding cell in a Uniform Manifold Approximation and Projection (UMAP) space. Further, each column was allowed to be standardized such that the sum of each column is 1. The two-dimensional UMAP projection was created using Pearson-residual normalized data[26] and default UMAP parameters implemented in the Seurat software package.[27] Then the smoothed expression matrix $\boldsymbol{S}_{markers\times cells}$ takes the form $\boldsymbol{S} = \boldsymbol{X}\boldsymbol{W}$

This smoothed expression matrix was clustered using k-means, and cells were subsequently assigned to an immune cell type based on the expression characteristics of the corresponding k-means cluster.

Plausible gene filtering using a contamination ratio metric

For spatial transcriptomic data, one major challenge is dealing with the impact of cell segmentation uncertainty, where even minor errors can potentially confound or distort downstream analyses. For cell-type specific analyses, we develop a "contamination ratio metric" for preemptively excluding genes which may be likely to return spurious results due to imperfect cell segmentation.[28]

Let $\bar{y}(t)_g$ denote the average expression of a particular gene g for a cell type t of interest. Further denote the average expression per cell of the gene in neighboring cells of other cell types by $\bar{y}\left(t'\right)_g$. Then the ratio

$$\psi_g = \frac{\bar{y}\left(t'\right)_g}{\bar{y}(t)_g}$$

Subcluster identification

To further refine cell types into distinct cell states or subclusters, we first identified for each cell type a list of genes that are plausibly expressed in that cell type to use for unsupervised subclustering. We defined this list of genes using the contamination ratio metric described above, selecting genes where the ratio metric $\psi_g < 1$. For a given cell type, this corresponds to subclustering using only genes with higher average expression within the cell type than in the spatially neighboring cells of other cell types. Unsupervised Louvain clustering was then performed among each cell type separately using only the filtered list of genes using Seurat.[27]

Spatial co-localization of cell states

Multinomial logistic regression was used to characterize differential spatial colocalization of cell states between patient groups. First, we identified for each patient all pairs of spatially neighboring cells within a 10 micron radius. Next, we performed multinomial logistic regression[29] separately for each possible cell state, estimating the probability of the neighboring cell state identity given patient group. Specifically, let Y_{in} denote the subcluster identity of the n^{th} neighbor to cell i. The regression model estimates $\Pr(Y_{in} = k | G_i)$, where G_i denotes the patient group of cell i (NR, PR, or CR), and k denotes cell state category.

For each modeled subcluster, we identified cell state pairs with differential colocalization probability between patient groups using the *emmeans* R package.[30]

Response group-specific ecosystems

First, a filter was applied to connections where Estimated Pr (neighbor subcluster) is greater in CR than in both NR and PR. Second a filter was applied to connections where at least one of the comparisons (CR vs NR) or (CR vs PR) is significant (p<5.9e−6). "Enriched in CR cells" indicates that the subcluster has significantly higher frequency in CR (p<0.05/98 subclusters) compared with NR and PR across all subclusters. The analogous filters were used to describe PR and NR response group ecosystems.

Validation with other single-cell data sets

Single-cell data sets were obtained from public repositories, and an overview of the external data sets and their characteristics is provided in online supplemental table 2. These data sets included an immune cell compendium from Domínguez Conde *et al*,[31] colon data from Kong *et al*,[32] breast cancer data from Bassez *et al*,[33] head and neck cancer data from Franken *et al*[34] and a large data set of 30 cancer types and their corresponding normal tissues from Kang *et al*.[35] The transfer functionality from the Seurat package was used to transfer CosMx cell types on these external data sets. Main cell types with a maximal prediction score <0.4 were considered unassigned. Cell subtypes were also considered unassigned if the parent cell type did not match that of the child cell type. Transfer of cell types was done for each data set separately. Cell type allocation in the current and external data were compared. For each cell (sub)type the overlap with the cell type in the external data was calculated as a percentage of all cells identified as a cell type as identified in the current study.

A paired Wilcoxon rank test was used to identify statistically significant differences between paired pretreatment and on-treatment samples in the triple negative breast cancer (TNBC) and head and neck squamous cell carcinoma (HNC) cohorts.[33 34] To identify differences in the ratio of cell types identified as supportive versus non-supportive for immunotherapy, the total number of supportive cells was divided by the total number of non-supportive cells. A positive ratio would indicate a higher fraction of supportive cells versus non-supportive cells. For a direct comparison of supportive cells versus non-supportive cells, we compared the percentages of supportive and non-supportive cells relative to the total number of cells measured in a patient.

RESULTS

Digital reconstruction of a vHSIL cell atlas shows high diversity across patients

FFPE vHSIL biopsies of 20 patients prior to immunotherapeutic vaccination who displayed a CR (n=6), PR (n=7) or NR (n=7)[10 11] (table 1) were analyzed at the single-cell transcriptomic level with the validated CosMx Spatial

Table 1 vHSIL cohort patient characteristics

CosMx study number	Trial study number	Diagnosis	Number of vaccine doses	Systemic T-cell response (MoM)	Clinical response at 3 months	Clinical response at 12 months	Trial reference
S10	206	vHSIL	4	16.5	CR	CR	NEJM
S17	503	vHSIL	4	245.5	CR	CR	CCR
S16	531	vHSIL	2	158.4	CR	CR	CCR
S12	532	vHSIL	2	207.4	CR	CR	CCR
S5	509	vHSIL	4	102	PR	CR	CCR
S11	563	vHSIL	3	178.7	PR	CR	CCR
S8	201	vHSIL	4	96.5	PR	PR	NEJM
S9	510	vHSIL	4	48.7	PR	PR	CCR
S13	512	vHSIL	4	78.2	PR	PR	CCR
S19	529	vHSIL	4	186.4	PR	PR	CCR
S18	530	vHSIL	3	195.3	PR	PR	CCR
S1	203	vHSIL	4	40.8	NR	PR	NEJM
S2	526	vHSIL	2	214	NR	PR	CCR
S15	228	vHSIL	4	61.4	NR	NR	NEJM
S7	519	vHSIL	4	194.5	NR	NR	CCR
S14	522	vHSIL	4	106.6	NR	NR	CCR
S6	524	vHSIL	4	68.1	NR	NR	CCR
S20	528	vHSIL	4	126.5	NR	NR	CCR
S3	202	vHSIL	4	2.9	NR	NR	NEJM
S4	517	vHSIL	4	161.5	NR	NR	CCR

NEJM reference:[10] Kenter *et al*.[10] *Vaccination against HPV-16 oncoproteins for vulvar intraepithelial neoplasia*. N Engl J Med, 361(19), 1838–1847. https://doi.org/10.1056/NEJMoa0810097
CCR reference:[11] Van Poelgeest *et al.*[11] *Vaccination against Oncoproteins of HPV16 for Non-invasive Vulvar/Vaginal Lesions: Lesion Clearance Is Related to the Strength of the T-Cell Response*. Clin Cancer Res, 22(10), 2342–2350. https://doi.org/10.1158/1078-0432.Ccr-15-2594
The MoM value was calculated by taking the median of the highest specific interferon-γ ELISpot counts against HPV16 E6 and E7 peptides per blood sample obtained during and after immunotherapeutic vaccination, so that one value could be obtained for the systemic T-cell response per individual patient.
CR, complete responders; ELISpot, enzyme-linked immunosorbent spot; HPV16, human papillomavirus type 16 ; MoM, median of maximum; NR, non-responders; PR, partial responders; vHSIL, vulvar high-grade squamous intraepithelial lesion.

Table 2 CosMx data metrics

	Complete responders	Partial responders	Non-responders	Full cohort
Number of fields of view	29	17	19	**65**
Area measured (mm^2)	16.43	9.63	10.76	**36.82**
Number of cells	121,877	62,573	90 428	**274,878**
Total transcripts	61,739,516	23,399,624	38,913,342	**124,052,482**
% of cells with >20 counts	98.08	97.45	98.13	**97.95**
Mean transcripts per cell	473	323	396	**413**
Assigned transcripts (%)	93.28	86.34	92.14	**91.61**
Genes detected above LOD	586	599	609	**611**
Cellular transcripts per μm^2	3.8	2.4	3.6	**3.4**
Mean negatives per cell	1.59	1.30	1.43	**1.47**

LOD, Limit of Detection.

Molecular Imager using a 1,000-plex RNA panel (online supplemental table 3).[19] A total of 65 fields of view with an accumulated area of >36 mm^2 resulted in the detection of 274,878 cells and a mean number of 413 transcripts detected per cell (table 2). Semi-supervised clustering of cells based on their RNA transcriptome (online supplemental table 4) resulted in the identification of 18 different cell types, including 6 types of epithelial cells, fibroblasts, endothelial cells, and several types of lymphocytes and myeloid cells (figure 1A, online supplemental figure 1A). Cell type neighborhood clustering revealed three epithelial, one stromal, and one stromal-epithelial interface spatial niches with roughly a similar cell count between all patients (figure 1B, online supplemental figure 1B,C).

The six different epithelial cell types were characterized based on their specific keratin expression[36] into basal cells, suprabasal cells, activated keratinocytes, contractile keratinocytes, differentiating and fully differentiated keratinocytes (online supplemental figure 1D,E). All together this allowed us to digitally reconstruct vHSIL lesions (figure 1CD). Moreover, we validated the concordance between keratin expression at the protein and gene transcript level (figure 1E). The proportion of each epithelial cell type present in the vHSIL lesion differed per patient, sustaining the notion that the disease manifests differently across patients, but no immunotherapy response-specific pattern was found (online supplemental figure 1F,G). This was also the case when the proportions of the other cell types were analyzed (online supplemental figure 1H). Thus, these data reveal vast heterogeneity between patients with a tumor that all had the same etiological background and originated in the same anatomical location.

Identification and validation of different cell states

To dissect the diversity of the different cell types within the TME and between patients, the non-epithelial cell types were further subclustered based on the set of genes higher expressed in that specific cell type when compared with all other cells (online supplemental table 4). This resulted in the identification of a total of 99 subclusters among endothelial cells (n=10), fibroblasts (n=10), CD4 T cells (n=11), CD8 T cells (n=8), regulatory T cells (Tregs; n=8), B cells (n=6), plasma cells (n=9), myeloid dendritic cells (mDCs; n=9), plasmacytoid DCs (pDC; n=6), macrophages (n=10), neutrophils (n=3), and mast cells (n=8) (online supplemental figure 2). To ascertain whether the cell (sub)types identified were specific for vHSIL, their presence was assessed in several publicly available data sets with large numbers of cells analyzed,[32 33 35] and an immune cell compendium[31] (online supplemental table 2). This not only successfully verified cell (sub)type identity (figure 2A, online supplemental figure 3) but also revealed that almost all identified immune cell subtypes in vHSIL were also present in other tissues, including a series of other healthy tissues and cancer types (online supplemental figure 4). The multiple different functional cell states of the cell types were derived by analysis of the cluster defining genes and literature (online supplemental table 5). Based on the comparison with the other data sets and marker gene expressions, some cell types were manually corrected (pDC_5, B cell_0 and 4, E_5), also showing that CD4_5 belonged to the Treg subclusters.

Balance between vaccine supportive and non-supportive cell states differs per clinical response

A comparison between the frequencies of the different cell types and their states in the lesions of CR, PR and NR patients was made to assess whether differences in clinical response were associated with the composition of the lesions before immunotherapy. This response group comparison revealed higher proportions of $CD8^+CD103^+$ tissue resident effector cells (CD8_6), $CD4^+CD161^+$ effector cells (CD4_6), phagocytic M1 macrophages (M_3), classically activated DCs (mDC_7), cDC2s (mDC_8), granzyme-B $(GZMB)^+$, interferon (IFN)-activated pDC (pDC_0), inflammatory mast cells (mast_1), T-cell infiltration supportive *IGFB7*hi endothelial cells[37] (E_8/9) and immunity supportive fibroblasts (F_2/3/4/5/8) among others in CR to immunotherapy (figure 2B).

In contrast, the lesions of PR comprised higher proportions of type 2 cytokine $CD4^+$ T cells (CD4_3, CD4_4) and *CCL18*-expressing macrophages (M_6), known to attract type 2 T cells and Tregs.[38–40] Non-responding lesions showed preferential infiltration with non-activated immune cells (CD8_3, CD4_0, M_0, mDC_4) and potentially suppressive fibroblasts (F_6/7/9) when compared with the other response groups (figure 2B).

For many subclusters, but not all, their transcriptome allowed us to propose a potential positive or negative direction of their effect on immunotherapy, based on our current knowledge of tumor-immunity (online supplemental table 5). The variation in the proportion of each individual cell type and cell state among the patients in each response group (online supplemental figure 5) suggested that rather than a difference in one specific cell type or cell state, it is the overall balance between the anticipated effect of all cell states present in the lesion that may influence clinical outcome. Indeed, while the proportions of cells with a supportive effect on immunotherapy were found in balance with the proportions of non-supportive cells in the CR group, the proportion of cells negatively impacting immunotherapy was higher in the PR and NR patient groups (figure 3). CR lesions exhibited a higher ratio of immune-supportive to immune-suppressive cells, compared with PR and NR lesions (figure 3).

Presence and response of detected immune cell states after immune checkpoint blockade

We identified two patient cohorts who received neoadjuvant checkpoint blockade therapy, of which single-cell transcriptomics data on all cell types present in the TME were available. In the first cohort, patients with TNBC

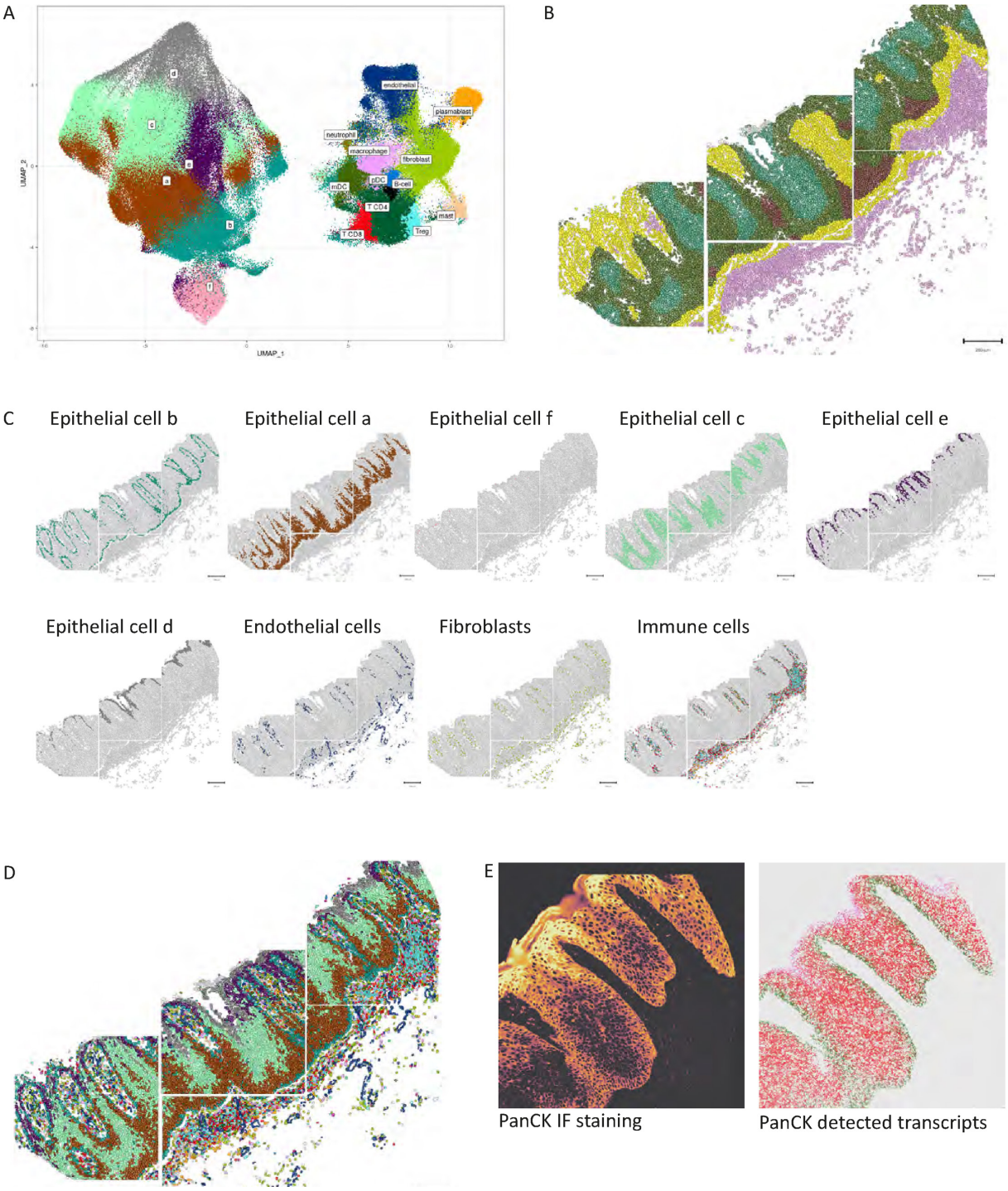

Figure 1 Cellular composition of vHSIL decomposed by spatial single-cell transcriptomics. Archived formalin-fixed, paraffin-embedded tissue sections obtained from vHSIL patients (n=20) before therapeutic vaccination with a human papillomavirus type 16 synthetic long peptide vaccine were subjected to single-cell spatial transcriptomics. On vaccination, six patients showed a complete response, seven a partial response and seven no response. (A) Uniform Manifold Approximation and Projection plot containing 274,878 cells resulted in the identification of 18 cell clusters. (B) Representative vHSIL CosMx image after cell segmentation and tissue segmentation, indicating the five spatial niches (three epithelial niches, one stromal niche, and one stroma-epithelium interface niche). (C) Representative images of the spatial location of different types of epithelial cells, fibroblasts, endothelial cells and different immune cells. (D) Full reconstruction of tissue section by spatially overlaying all cell clusters. (E) Comparison of pan-cytokeratin (PanCK) protein detection by immunofluorescence (antibody clone NB2-33200AF532, Novus) and RNA detection, showing a good overlay between protein and RNA detection. IF, immunofluorescence; vHSIL, vulvar high-grade squamous intraepithelial lesions.

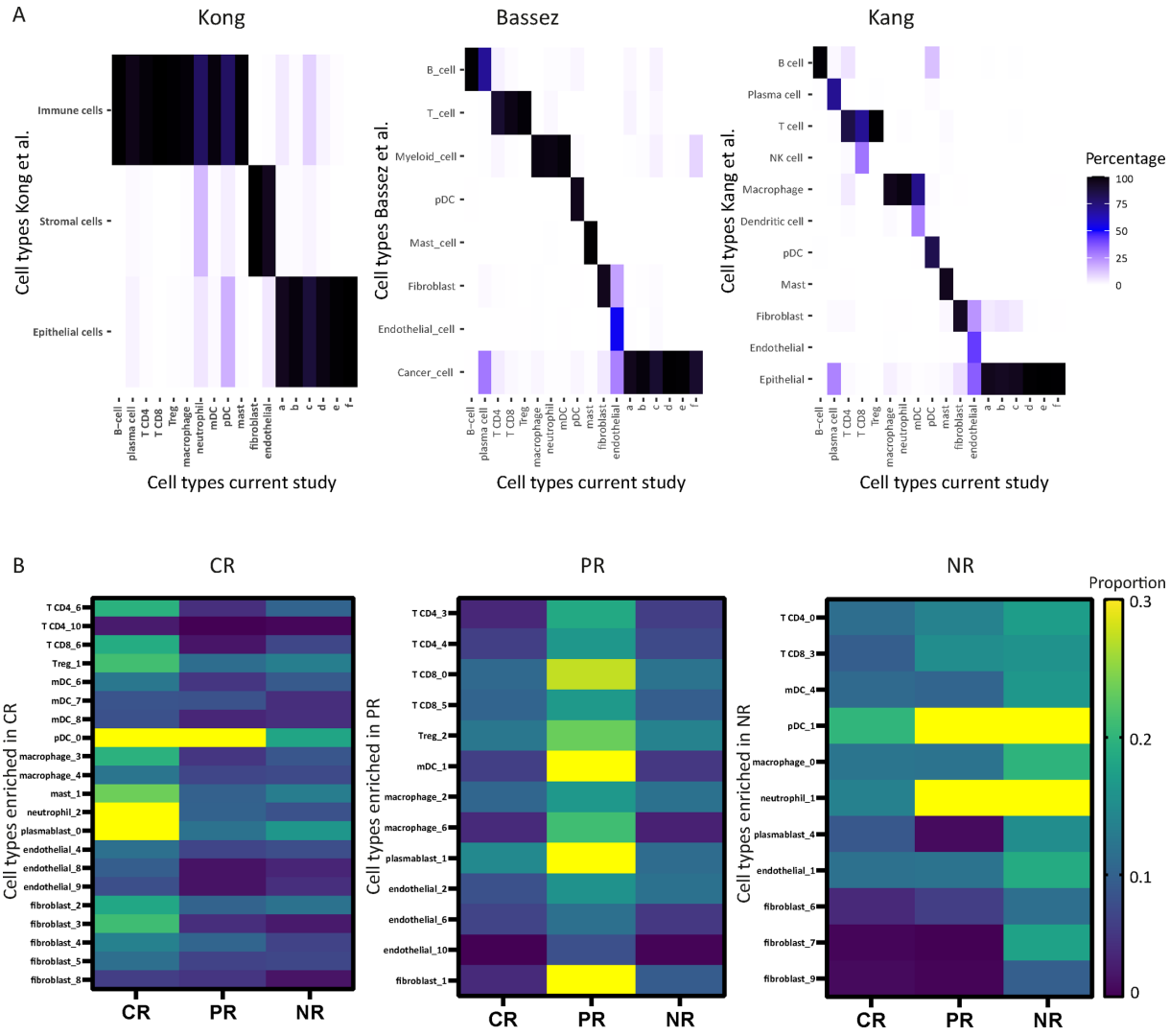

Figure 2 Validation of cell types and cell states specific for clinical response to immunotherapeutic vaccination. (A) To validate the existence of the identified 18 cell clusters, their transcriptome was compared with large numbers of single cells present in several publicly available data sets: Kong *et al*,[32] Bassez *et al*[33] and Kang *et al*,[35] showing high concordance between the identified cell clusters in this study versus that of the public databases. (B) Heatmaps showing the cell states that are specifically enriched (Z-test for difference in proportion, Bonferroni corrected) in complete responders (CR, n=6), partial responders (PR, n=7) and non-responders (NR, n=7) therapeutic vaccination, and compared with their presence in the other response groups. The color legend indicates the proportion of each cell state within the major cell type. The explanation of the cell type abbreviations can be found in online supplemental table 5. mDC, myeloid dendritic cell; NK, natural killer; pDC, plasmacytoid dendritic cell; Treg, regulatory T cell.

were treated with anti-programmed cell death protein-1 (PD-1) prior to surgery.[33] In the second cohort, the effect of neoadjuvant anti-programmed death-ligand 1 (PD-L1) with or without anti-cytotoxic T-lymphocyte associated protein 4 (CTLA-4) was studied in advanced resectable HNC.[34] We interrogated these data sets for the presence and response to checkpoint blockade of the immune cell states detected in the vHSIL lesions by a comparison of the frequencies of all these cells in the TME before neoadjuvant checkpoint therapy and at surgery.

In both cohorts, checkpoint blockade resulted in the increased detection of the immune supportive $CD4^+CD161^+$ effector cells (CD4_6) and activated chemotactic $CD8^+$ cells (CD8_7), while a decrease was observed in the non-supportive population of suppressive $CD8^+$ cells (CD8_0) (figure 4AB). In addition, in both cohorts, a decreased presence of non-supportive fibroblasts (F_1, F_6, F_7) was observed (figure 4AB). There were also treatment group-specific changes in immune supportive and non-supportive cell states found. In the TNBC cohort, an increase in immune supportive proliferating $CD4^+$ cells (CD4_9) and chemotactic macrophages (M_5) was observed after checkpoint blockade, while for the immune non-supportive populations an increase in Tregs (Treg_1, Treg_4) and a decrease in CD8_3 cells was found (figure 4AB). In the HNC cohort, the decrease of DC-like macrophages (mDC_3) and *IGFB7*$^+$ endothelial cells (E_8) was observed after treatment (figure 4AB).

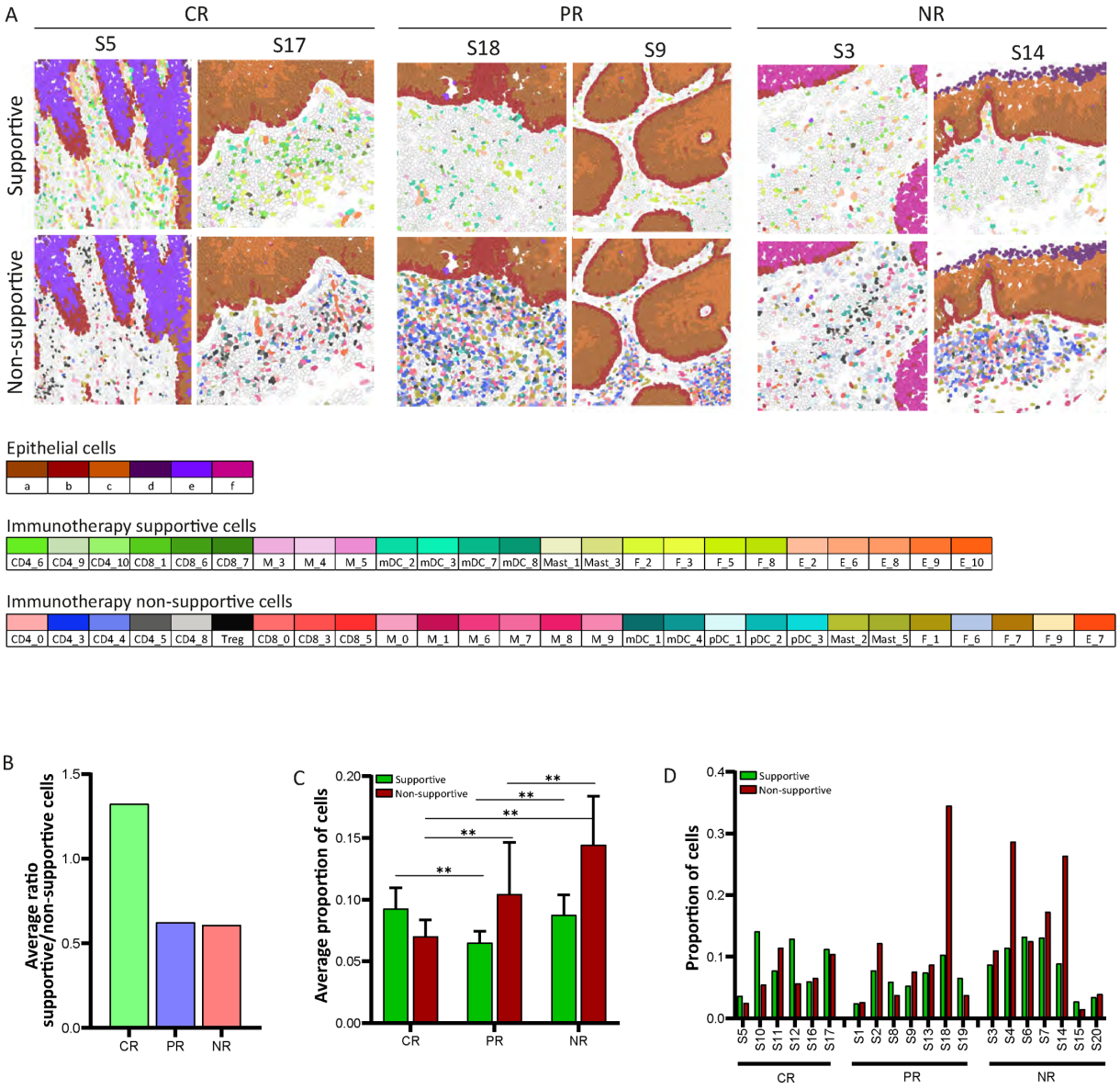

Figure 3 The balance between vaccination supportive and non-supportive cells differs per vaccine response group. For many subclusters, their transcriptome allowed identifying them as potentially supportive or non-supportive for immunotherapy (online supplemental table 5). Cells classified as supportive were: CD4_6/9/10; CD8_1/6/7; M_2/3/4/5; mDC_2/3/7/8; pDC_4; Mast_1/3; F_2/3/5/8; E_2/6/8/9/10. Cells classified as non-supportive were: CD4_0/3/4; Tregs; CD8_0/3/5; mDC_1/4; M2_0/1/6/7/8/9; pDC_1/2/3; Mast _2/5; F_1/6/7/9; E_7. The explanation of the cell type abbreviations can be found in online supplemental table 5. (A) Two representative CosMx images per response group in which the immunotherapy supportive cells (upper image) and the immunotherapy non-supportive cells (lower image) are visualized in situ. Epithelial cells are also shown for reference. (B) The ratio of therapeutic vaccine supportive versus non-supportive cells was determined in complete responders (CR), partial responders (PR) and non-responders (NR) to therapeutic vaccination. Ratio >1 indicating an excess of supportive cells, <1 indicating an excess of non-supportive cells. (C) The average proportion of total cells classified either as supportive (green) or non-supportive (red) in the groups of CR, PR and NR patients. Statistical significance is calculated with the Z-test for difference in proportion and indicated with asterisks: *p<0.05, **p<0.01 and ***p<0.001. (D) The proportion of total cells classified either as supportive (green) or non-supportive (red), present per individual patient. CR, n=6, PR, n=7, NR, n=7. mDC, myeloid dendritic cell; pDC, plasmacytoid dendritic cell; Treg, regulatory T cell.

The consistent increase in $CD4^+CD161^+$ effector cells (CD4_6), the activated chemotactic $CD8^+$ cells (CD8_7) and decrease in the non-supportive population of suppressive $CD8^+$ cells (CD8_0) single these cell states out as cells that are particularly being modulated by immune checkpoint therapy, irrespective of the checkpoint blocking antibody used. However, tumor type-specific and/or therapy-specific changes in immune supportive and non-supportive cell states were also found. To assess whether checkpoint therapy displayed an overall positive effect on the proportion of immune-supportive cells in the TME, we interrogated the data of these two cohorts with respect to the balance between immunotherapy-supportive

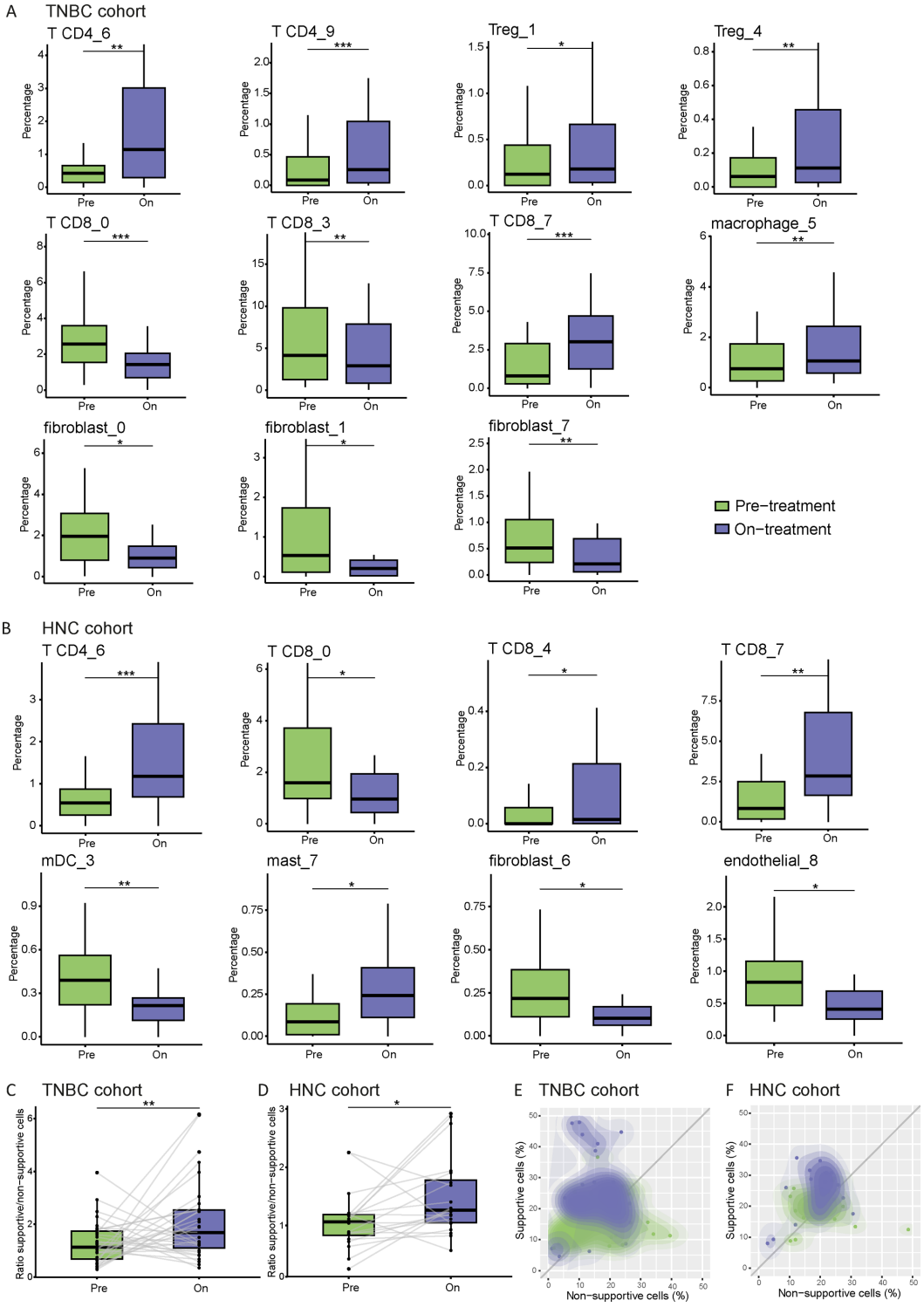

Figure 4 The response of identified cell states on checkpoint blockade. Neoadjuvant checkpoint blockade altered the proportion of several of the identified cell states present in the TME of (A) patients with triple negative breast cancer (TNBC),[33] and (B) patients with advanced resectable head and neck squamous cell carcinoma (HNC).[34] Boxplots show the proportion of those cells that significantly shifted after checkpoint blockade. The ratio of immunotherapy supportive versus non-supportive cells was determined in (C) the TNBC cohort and (D) in the HNC cohort, before and after checkpoint blockade therapy. Boxplots depict this ratio and how it changes on immunotherapy, with paired patient data (lines connecting the same patient). Statistical significance is calculated with the Wilcoxon rank test and indicated with asterisks: *p<0.05, **p<0.01 and ***p<0.001. The explanation of the cell type abbreviations can be found in online supplemental table 5. (E, F) The shift in the proportion of immunotherapy supportive and non-supportive cells before and after checkpoint blockade was visualized by scatter plots, showing a specific increase in the proportion of immunotherapy supportive cells on checkpoint blockade therapy (vertical shift of the cloud on therapy), while the proportion of non-supportive cells did not change on therapy (no horizontal shift). mDC, myeloid dendritic cell; Treg, regulatory T cell.

and non-supportive cells. In both cohorts, the ratio between supportive and non-supportive cell states increased, indicating a shift towards a higher presence of immune-supportive cells in the TME after checkpoint blockade (figure 4C,D). Scatter plots showing the percentage of all supportive and non-supportive cell states in the TME for the patients before and after checkpoint blockade therapy show a treatment-associated shift upwards above the diagonal, indicating that the enhanced ratio mostly is due to an increased percentage of immune supportive cell states on treatment (figure 4E,F). Overall, these data indicate that checkpoint blockade is associated with significant alteration of the TME in favor of effective antitumor immunity and suggests a more prominent role for the $CD4^+CD161^+$ effector cells (CD4_6) and the activated chemotactic $CD8^+$ cells (CD8_7) in this treatment.

Spatial ecosystems prime the patient's clinical response to immunotherapy

The abundance of specific cell states from a variety of cell types in each response group can reflect different functional ecosystems in which different cells may play a role to build the ecosystem and/or interact to achieve a particular functional outcome within the ecosystem. We performed a 10 µm distance neighborhood analysis to capture potential interactions between cells that were significantly enriched in one clinical response group when compared with the other two response groups of vHSIL patients. In the CR group, a central role was found for *CXCL14*$^+$ reticular fibroblasts (F_3), known to foster immune cell infiltration,[41] displaying clustering with many types of T cells and dendritic cells (figure 5A, online supplemental figure 6A). CXCL14 is a chemokine with both protumor (inducing M2 proliferation of macrophages, stimulating angiogenesis) and antitumor (chemotaxis of dendritic cells and natural killer cells) capacities, depending on the context.[42–44] High numbers of *CXCL14*-expressing fibroblasts have previously been found to be associated with response to immune checkpoint blockade in renal cell carcinoma[45] and with improved antitumor immunity in glioma.[46] Moreover, there was an enrichment of multiple specific cell states, including that of effector T cells (CD4_6; CD8_6), phagocytic macrophages (M_3), pDC_0, Tregs and of a T-cell infiltrating supporting endothelial (E_8) subset[37] more preferentially present in the CR than in the PR and NR group and with a higher probability to form the ecosystem (figure 5).

In the PR group, a central role was found for two CD4 cell states (CD4_3 and CD4_4) interacting with many different states of dendritic cells and macrophages (figure 5B). In particular, two $CD4^+$ T cell states associated with type 2 cytokine production clustered at higher probability with *CCL18*-expressing (M_6) macrophages, fibroblasts_1, suppressive mDC_1 and Tregs (CD4_5 and Tregs) compared with patients with CR or NR (figure 5). As literature shows that especially CCL18+macrophages activate fibroblasts,[47 48] we investigated the correlation between the *CCL18*+macrophages (M_6) and fibroblasts. Indeed, a direct relationship was found between the presence of *CCL18*+macrophages (M_6) and fibroblasts in PR patients (r=0.97, p=0.0003), but not in NR (r=−0.17, p=0.71) or CR (r=−0.24, p=0.65) (online supplemental figure 6B). Yet, when the correlation between macrophage_6 and the various fibroblast subtypes was examined, we found that the presence of *CCL18*+macrophages was specifically related to the presence of the fibrosis-enhancing subtype fibroblasts_1 in all response groups (PR, r=0.95, p=8.7×10−4; NR, r=0.86, p=0.01; CR, r=0.79, p=0.06) but most pronounced in the PR patient group (online supplemental figure 6C) and fitting with the fact that this patient group displayed the strongest influx of *CCL18*+macrophages. This confirms that CCL18, but in particular CCL18-expressing macrophages being the most dominant cell type expressing *CCL18* (online supplemental figure 6D), induce immunosuppressive fibroblasts.

The CR-specific and PR-specific spatial ecosystems clearly differed from the one found in the NR group, as in the latter group specific enrichment of interactions between non-supportive fibroblasts (F_6) and macrophages (M_0) and Tregs was found (figure 5). These data demonstrate the presence of specific spatial ecosystems in vHSIL, of which the organization of tumor-immunity supporting cell clusters in CR clearly differs from the predominantly type 2 cytokine response-supporting cell clusters organized in PR, and from the absence of specific immune cell clusters in NR. This suggests that the type of cellular ecosystem present in treatment-naïve vHSIL supports or restrains the clinical response to immunotherapeutic vaccination. Analysis of two pre-vaccination and post-vaccination vHSIL biopsies sustained this notion, showing an increased Th2 and a decreased Th1 outgrowth in a PR patient, but not in a CR patient, despite a similar strong systemic vaccine-induced IFN-γ response mediated predominantly by CD4 T cells (online supplemental figure 7).

DISCUSSION

Leveraging single-cell spatial transcriptomics in a clinically driven approach, we addressed a fundamental question in cancer research: the complexity and heterogeneity of the TME and its impact on immunotherapy responsiveness. Our analysis revealed that the complexity and diversity of cellular states in the TME varies significantly between patients, even among those with similar clinical outcomes. Specifically, the proportion of cells potentially supportive or non-supportive to antitumor immunity differs across patients and there was no consistent association between specific cell types and clinical response to immunotherapeutic vaccination. Instead, the TME of patients who achieved CR displayed a specific ecosystem in which inflammatory cells capable of supporting vaccine-driven antitumor responses closely interacted. In

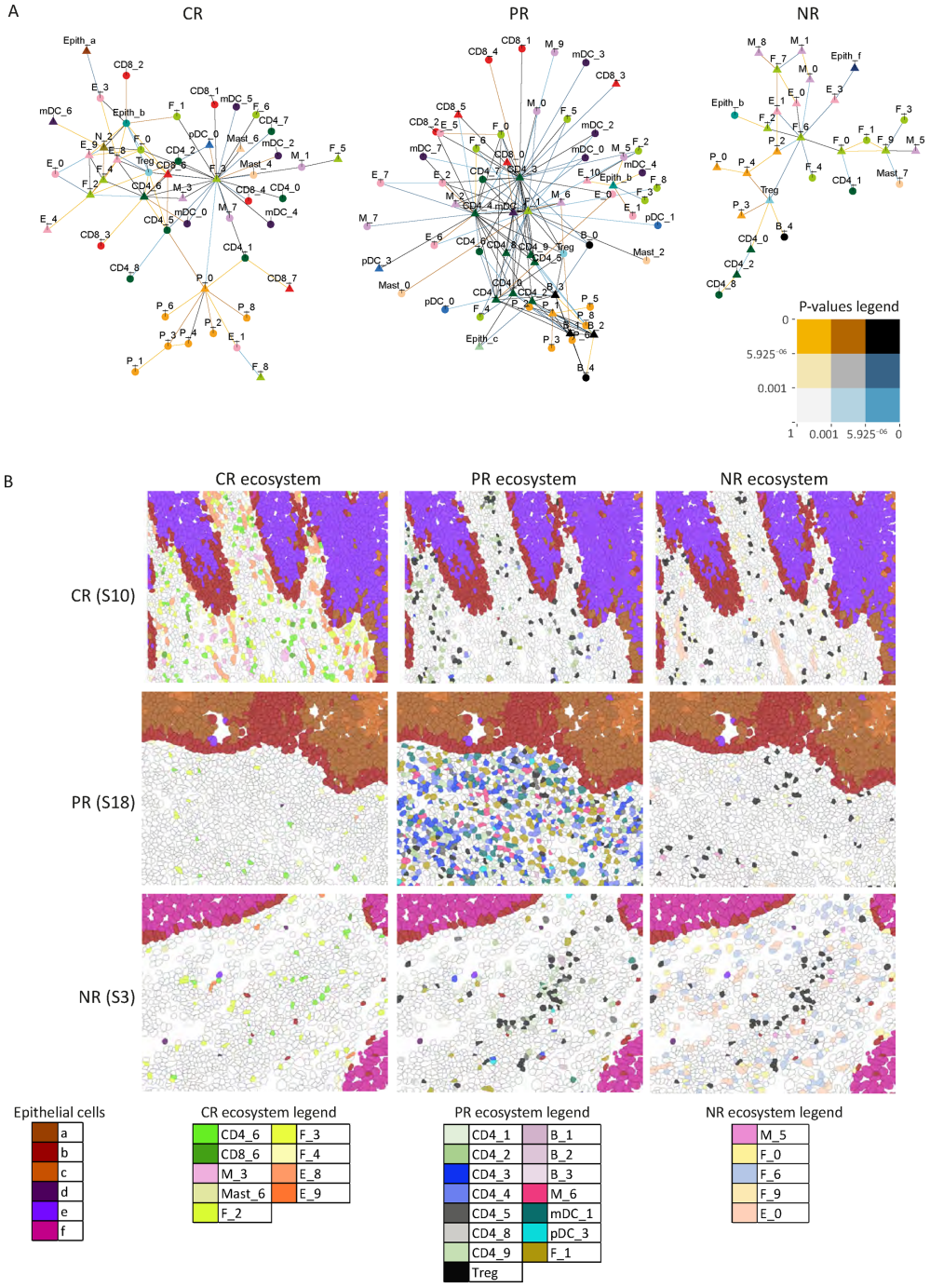

Figure 5 Pre-existing cellular ecosystems are specific for the response to therapeutic vaccination. To capture potential cellular interactions, a 10 µm distance neighborhood analysis was performed on the single-cell spatial transcriptomics data of the complete responders (CR, n=6), partial responders (PR, n=7) and non-responders (NR, n=7) in the vHSIL cohort treated with therapeutic vaccination. (A) Spatial cellular interaction networks ("ecosystems") that are specific for therapeutic vaccine-induced CR, PR and NR are shown. A triangle indicates cell types with a cell frequency that is specifically enriched in that response group, a circle indicates those that are not specifically enriched. The color of the connecting line reflects the level of significance and indicates how prominent the spatial interaction is in that response group, calculated by multinomial logistic regression (comparing the connection for pairs of subclusters between groups). The legend for the corresponding p values is provided as a colored box. For CR: The orange line indicates significantly increased compared with PR, and the blue line indicates significantly increased compared with NR. For PR: The orange line indicates significantly increased compared with NR, and the blue line indicates significantly increased compared with CR. For NR: The orange line indicates significantly increased compared with PR, and the blue line indicates significantly increased compared with CR. (B) Visualization of the cells forming the CR, PR or NR characteristic ecosystems in a representative CR, PR and NR formalin-fixed, paraffin-embedded vHSIL section. Epithelial cells are also shown for reference. The explanation of the cell type abbreviations can be found in online supplemental figure 5. vHSIL, vulvar high-grade squamous intraepithelial lesions. mDC, myeloid dendritic cell; pDC, plasmacytoid dendritic cell; Treg, regulatory T cell.

PR, the TME comprised a mixed type 1 and type 2 cellular environment which was specifically dominated by close interactions between type 2 immune cells, generally less effective at supporting antitumor immunity.[49] Our findings also show that neoadjuvant immune checkpoint therapy altered the balance between immune-supportive and non-supportive cell states within the TME, specifically increasing the proportion of immune-supportive cells. These observations underscore the broader clinical relevance of our data.

This study investigates the TME of patients treated with an immunotherapeutic vaccine. Over five decades of research have driven substantial progress in therapeutic cancer vaccine development, including the improved identification of tumor-specific antigens, the engineering of highly immunogenic platforms, and the integration of vaccines with immune checkpoint blockade therapies. These advancements are now bolstered by reliable methods for assessing vaccine pharmacodynamics.[1 50] Despite these innovations, the identification of robust predictive biomarkers for clinical success remains a pivotal unmet need. While vaccine-induced immune responses often correlate with clinical activity in trials,[1 17 50–53] pinpointing specific cellular or molecular biomarkers has proven challenging. This is likely due to the complexity and heterogeneity of the TME, where cell types, cell states, and their spatial interactions exhibit significant interpatient heterogeneity. Our findings underscore the importance of analyzing the TME in its spatial context to unravel this complexity. This spatially informed perspective may transform how we evaluate and stratify patients in immunotherapy, enabling tailored interventions with greater clinical impact.

Our data suggest that the overall balance between immune-supportive and restraining cells in the TME—spanning lymphocytes, myeloid cells, fibroblasts, and endothelial cells—determines vaccine efficacy. Moreover, our findings indicate that distinct cellular ecosystems, rather than isolated cell types, govern the lesion's susceptibility to immunotherapeutic vaccination. An ideal therapeutic vaccine amplifies tumor-specific type 1 cytokine-producing CD4+ and CD8+ T cells.[1 54] However, PR patients exhibited ecosystems enriched with type 2 cytokine-producing CD4+T cells (CD4_3, CD4_4), which interacted with Th2-attracting macrophages (M_6), wound-healing fibroblasts (F_1), and certain dendritic cells (mDC_1). This Th2-dominant environment may undermine vaccine-driven antitumor responses, despite the presence of robust systemic Th1/Th2 immunity post-vaccination.[17]

The presence of distinct ecosystems explaining variable clinical outcomes is consistent with observations in preclinical and clinical models. For example, recent murine studies demonstrated that a spatial triad of CD4+T cells, CD8+T cells, and dendritic cells is critical for both antitumor immunity and responsiveness to checkpoint inhibitors.[55] Similarly, Luca *et al* identified carcinoma ecosystems (CEs) across 16 human cancers.[56] Two distinct ecosystems, CE9 and CE10, have been strongly associated with favorable clinical outcomes, including longer overall survival, spontaneous regression of premalignant lung lesions (CE10), and positive responses to checkpoint blockade therapy (CE9). The differential association of CE9 and CE10 with specific clinical outcomes underscores the concept of therapy-specific ecosystems. Consistent with this, the CR-associated ecosystem identified in our study shares several cellular states with CE9 and CE10. For example, DC_S1 and mDC_2 correspond to cDC1; DC_S3 (CD80, CD274) aligns with mDC_7; CD8_S1 (GZMK) matches CD8_3; CD8_S3 (GZMB) is similar to CD8_6; Mast S4 (TPSAB1, TPSB2, CPA3) corresponds to Mast_1; CD4_S1 (IL-2RA, CTLA-4, Foxp3, TIGIT) resembles Tregs/CD4_5; and CD4_S2 (IL-7R) aligns with CD4_6. Importantly, our findings also revealed the enriched presence of cDC2 (mDC_8), phagocytic M1 macrophages (M_3), a unique fibroblast state (F_3), and several IGFBP7^{hi} endothelial cell states in CR patients, further illustrating ecosystem-level differences linked to clinical outcomes.

These results extend our understanding of T cell-based immunotherapy, highlighting conserved cellular features across various treatment modalities. One prominent example is the enrichment of CD161(KLRB1)+CD4+ Th1 effector cells in CR patients from our vaccine cohort. This cell population was similarly enriched in responders with TNBC and HNC treated with PD-1 or PD-L1 checkpoint blockade.[33 34] Our previous work described this CD161+CD4+ effector memory subset in tumors exhibiting active antitumor T-cell responses.[57] These cells are characterized by their ability to produce key effector cytokines, including IFN-γ and tumor necrosis factor-α,[16] and their rapid response to antigen recognition compared with CD161-negative counterparts.[58] Moreover, increased numbers of intratumoral CD161+CD4+ effector cells are strongly correlated with improved survival in multiple cancers, including HNC.[16 58] Collectively, these observations underscore the pivotal role of this CD4+T cell population in driving effective immunotherapy responses.

Another key finding is the presence of cells producing immune cell homing cytokines, which were detected in both PR and CR. Specifically, we identified a subset of CD4+T cells (CD4_2) expressing interleukin-16, a cytokine known to recruit monocytes, dendritic cells, and T cells into lesions.[59–61] In vHSIL, CD4_2 cells were spatially interacting with effector cells, including CD4_6 and CD8_6. In checkpoint blockade cohorts, treatment increased the prevalence of CD8+T cells (CD8_7) producing the chemokines CCL3 and CCL4, which attract various myeloid cell types and T cells.[62 63] Recent evidence also demonstrates that CCL3 and CCL4-producing CD8+T cells infiltrate tumors on therapeutic vaccination, driving the recruitment and activation of phagocytic M1-like macrophages, ultimately leading to complete tumor regression.[64] Based on their cellular interactions within the CR ecosystem and functional roles described in the literature, several other cell

states are likely to positively influence clinical outcomes following immunotherapy. While the contribution of these states remains to be fully elucidated, the importance of CD161+Th1 cells (CD4_6), chemotactic CD8+T cells (CD8_7), CD8+CD103+ tissue-resident effector cells (CD8_6), and phagocytic M1 macrophages (M_3) has been firmly established.[65]

The study also identified macrophages expressing *CCL18*, a marker of alternatively activated macrophages within Th2-dominant environments.[66] While CCL18 may directly boost tumor growth,[67] its production also leads to the preferential attraction of Th2-like cells and Tregs,[39 40] both enriched in PR patients. The presence of these macrophages was connected to that of Th2 cells, both of which were predominantly found in patients with a PR on therapeutic vaccination. Previously, we have shown that vaccination led to the activation of both Th1 and Th2 CD4+T cells, and in a vHSIL patient case with a PR, we were able to show that only tumor-specific Th2 cells could be cultured from the lesion after vaccination.[17] Our study thus identified CCL18 as a potential target for co-treatment during therapeutic vaccination. A recently developed in vivo active CCL18 blocking peptide[68] may provide such help.

X Roderick C Slieker @rcslieker

Contributors Conceptualisation: ZA, SHvdB. Formal analysis: ZA, RCS, DM. Resources: MJPW, MIEvP. Supervision: SHvdB. Funding acquisition: ZA, SHvdB. Writing original draft: ZA, SHvdB. Writing review: ZA, RCS, DM, MJPW, MIEvP, SHvdB. Guarantor: SHvdB.

Funding ZA received an MD/PhD grant from Leiden University Medical Center. SHvdB received base funding from Oncode Institute and support from Oncode Accelerator, a Dutch National Growth Fund project under grant number NGFOP2201.

Competing interests No, there are no competing interests.

Patient consent for publication Not applicable.

Ethics approval The study was conducted in accordance with the Declaration of Helsinki and approved by the national Central Committee on Research Involving Human Subjects (CCMO, NL21215.000.08) and the Leiden University Medical Center institutional ethical committee (P08.197). Participants gave informed consent to participate in the study before taking part.

Provenance and peer review Not commissioned; externally peer reviewed.

Data availability statement Data are available in a public, open access repository. Data are available upon reasonable request. All data relevant to the study are included in the article or uploaded as supplementary information. All data generated during this study are included in this article and are provided on https://github.com/rodericksliecker/CosMx_vHSIL, and are available upon reasonable request.

ORCID iDs
Ziena Abdulrahman http://orcid.org/0000-0001-9079-0293
Sjoerd H van der Burg http://orcid.org/0000-0002-6556-0354

REFERENCES

1 Saxena M, van der Burg SH, Melief CJM, *et al*. Therapeutic cancer vaccines. *Nat Rev Cancer* 2021;21:360–78.
2 Rosenberg SA, Restifo NP. Adoptive cell transfer as personalized immunotherapy for human cancer. *Science* 2015;348:62–8.
3 Zappasodi R, Merghoub T, Wolchok JD. Emerging Concepts for Immune Checkpoint Blockade-Based Combination Therapies. *Cancer Cell* 2018;33:581–98.
4 Binnewies M, Roberts EW, Kersten K, *et al*. Understanding the tumor immune microenvironment (TIME) for effective therapy. *Nat Med* 2018;24:541–50.
5 Bruni D, Angell HK, Galon J. The immune contexture and Immunoscore in cancer prognosis and therapeutic efficacy. *Nat Rev Cancer* 2020;20:662–80.
6 Helmink BA, Reddy SM, Gao J, *et al*. B cells and tertiary lymphoid structures promote immunotherapy response. *Nature New Biol* 2020;577:549–55.
7 Wang XQ, Danenberg E, Huang C-S, *et al*. Spatial predictors of immunotherapy response in triple-negative breast cancer. *Nature New Biol* 2023;621:868–76.
8 Bill R, Wirapati P, Messemaker M, *et al*. *CXCL9:SPP1* macrophage polarity identifies a network of cellular programs that control human cancers. *Science* 2023;381:515–24.
9 Abdulrahman Z, Santegoets SJ, Sturm G, *et al*. Tumor-specific T cells support chemokine-driven spatial organization of intratumoral immune microaggregates needed for long survival. *J Immunother Cancer* 2022;10:e004346.
10 Kenter GG, Welters MJP, Valentijn ARPM, *et al*. Vaccination against HPV-16 oncoproteins for vulvar intraepithelial neoplasia. *N Engl J Med* 2009;361:1838–47.
11 van Poelgeest MIE, Welters MJP, Vermeij R, *et al*. Vaccination against Oncoproteins of HPV16 for Noninvasive Vulvar/Vaginal Lesions: Lesion Clearance Is Related to the Strength of the T-Cell Response. *Clin Cancer Res* 2016;22:2342–50.
12 Lee J, Nicosia M, Hong ES, *et al*. Sex-Biased T-cell Exhaustion Drives Differential Immune Responses in Glioblastoma. *Cancer Discov* 2023;13:2090–105.
13 Spranger S, Bao R, Gajewski TF. Melanoma-intrinsic β-catenin signalling prevents anti-tumour immunity. *Nature New Biol* 2015;523:231–5.
14 Peng W, Chen JQ, Liu C, *et al*. Loss of PTEN Promotes Resistance to T Cell–Mediated Immunotherapy. *Cancer Discov* 2016;6:202–16.
15 Liu C, Peng W, Xu C, *et al*. BRAF Inhibition Increases Tumor Infiltration by T cells and Enhances the Antitumor Activity of Adoptive Immunotherapy in Mice. *Clin Cancer Res* 2013;19:393–403.
16 Santegoets SJ, van Ham VJ, Ehsan I, *et al*. The Anatomical Location Shapes the Immune Infiltrate in Tumors of Same Etiology and Affects Survival. *Clin Cancer Res* 2019;25:240–52.
17 Welters MJP, Kenter GG, de Vos van Steenwijk PJ, *et al*. Success or failure of vaccination for HPV16-positive vulvar lesions correlates with kinetics and phenotype of induced T-cell responses. *Proc Natl Acad Sci U S A* 2010;107:11895–9.
18 Abdulrahman Z, de Miranda N, van Esch EMG, *et al*. Pre-existing inflammatory immune microenvironment predicts the clinical response of vulvar high-grade squamous intraepithelial lesions to therapeutic HPV16 vaccination. *J Immunother Cancer* 2020;8:e000563.
19 He S, Bhatt R, Brown C, *et al*. High-plex imaging of RNA and proteins at subcellular resolution in fixed tissue by spatial molecular imaging. *Nat Biotechnol* 2022;40:1794–806.
20 Hornburg M, Desbois M, Lu S, *et al*. Single-cell dissection of cellular components and interactions shaping the tumor immune phenotypes in ovarian cancer. *Cancer Cell* 2021;39:928–44.
21 Zilionis R, Engblom C, Pfirschke C, *et al*. Single-Cell Transcriptomics of Human and Mouse Lung Cancers Reveals Conserved Myeloid Populations across Individuals and Species. *Immunity* 2019;50:1317–34.
22 Zhang Y, Chen H, Mo H, *et al*. Single-cell analyses reveal key immune cell subsets associated with response to PD-L1 blockade in triple-negative breast cancer. *Cancer Cell* 2021;39:1578–93.
23 Maier B, Leader AM, Chen ST, *et al*. A conserved dendritic-cell regulatory program limits antitumour immunity. *Nature New Biol* 2020;580:257–62.

24 Wang Y, Zhao J, Xu H, *et al*. A systematic evaluation of computational methods for cell segmentation. *Brief Bioinformatics* 2024;25:e407.
25 Danaher P, Zhao E, Yang Z, *et al*. Insitutype: likelihood-based cell typing for single cell spatial transcriptomics. *Bioinformatics* [Preprint] 2022.
26 Lause J, Berens P, Kobak D. Analytic Pearson residuals for normalization of single-cell RNA-seq UMI data. *Genome Biol* 2021;22:258.
27 Butler A, Hoffman P, Smibert P, *et al*. Integrating single-cell transcriptomic data across different conditions, technologies, and species. *Nat Biotechnol* 2018;36:411–20.
28 Vasconcelos AG, McGuire D, Simon N, *et al*. Differential expression analysis for spatially correlated data. *Genomics* [Preprint] 2024.
29 Venables WNRipley B. Modern Applied Statistics with S. Statistics and Computing. New York: Springer, 2002.
30 Lenth R. *Emmeans: Estimated Marginal Means, Aka Least-Squares Means*. . R Package Version, 2022:1. 2.
31 Domínguez Conde C, Xu C, Jarvis LB, *et al*. Cross-tissue immune cell analysis reveals tissue-specific features in humans. *Science* 2022;376:eabl5197.
32 Kong L, Pokatayev V, Lefkovith A, *et al*. The landscape of immune dysregulation in Crohn's disease revealed through single-cell transcriptomic profiling in the ileum and colon. *Immunity* 2023;56:444–58.
33 Bassez A, Vos H, Van Dyck L, *et al*. A single-cell map of intratumoral changes during anti-PD1 treatment of patients with breast cancer. *Nat Med* 2021;27:820–32.
34 Franken A, Bila M, Mechels A, *et al*. CD4$^+$ T cell activation distinguishes response to anti-PD-L1+anti-CTLA4 therapy from anti-PD-L1 monotherapy. *Immunity* 2024;57:541–58.
35 Kang J, Lee JH, Cha H, *et al*. Systematic dissection of tumor-normal single-cell ecosystems across a thousand tumors of 30 cancer types. *Nat Commun* 2024;15:4067.
36 Freedberg IM, Tomic-Canic M, Komine M, *et al*. Keratins and the keratinocyte activation cycle. *J Invest Dermatol* 2001;116:633–40.
37 Li Q, Shao S, Zhu Z, *et al*. An IGFBP7hi endothelial cell subset drives T cell extravasation in psoriasis via endothelial glycocalyx degradation. *J Clin Invest* 2023;133:e160451.
38 Islam SA, Ling MF, Leung J, *et al*. Identification of human CCR8 as a CCL18 receptor. *J Exp Med* 2013;210:1889–98.
39 de Nadaï P, Charbonnier A-S, Chenivesse C, *et al*. Involvement of CCL18 in allergic asthma. *J Immunol* 2006;176:6286–93.
40 Chenivesse C, Chang Y, Azzaoui I, *et al*. Pulmonary CCL18 recruits human regulatory T cells. *J Immunol* 2012;189:128–37.
41 Lu J, Chatterjee M, Schmid H, *et al*. CXCL14 as an emerging immune and inflammatory modulator. *J Inflamm (Lond)* 2016;13:1.
42 Augsten M, Hägglöf C, Olsson E, *et al*. CXCL14 is an autocrine growth factor for fibroblasts and acts as a multi-modal stimulator of prostate tumor growth. *Proc Natl Acad Sci U S A* 2009;106:3414–9.
43 Augsten M, Sjöberg E, Frings O, *et al*. Cancer-Associated Fibroblasts Expressing CXCL14 Rely upon NOS1-Derived Nitric Oxide Signaling for Their Tumor-Supporting Properties. *Cancer Res* 2014;74:2999–3010.
44 Hara T, Tanegashima K. Pleiotropic functions of the CXC-type chemokine CXCL14 in mammals. *J Biochem* 2012;151:469–76.
45 Pan Q, Liu R, Zhang X, *et al*. CXCL14 as a potential marker for immunotherapy response prediction in renal cell carcinoma. *Ther Adv Med Oncol* 2023;15:17588359231217966.
46 Kumar A, Mohamed E, Tong S, *et al*. CXCL14 Promotes a Robust Brain Tumor-Associated Immune Response in Glioma. *Clin Cancer Res* 2022;28:2898–910.
47 Zeng W, Xiong L, Wu W, *et al*. CCL18 signaling from tumor-associated macrophages activates fibroblasts to adopt a chemoresistance-inducing phenotype. *Oncogene* 2023;42:224–37.
48 Lin L, Chen Y-S, Yao Y-D, *et al*. CCL18 from tumor-associated macrophages promotes angiogenesis in breast cancer. *Oncotarget* 2015;6:34758–73.
49 Fridman WH, Pagès F, Sautès-Fridman C, *et al*. The immune contexture in human tumours: impact on clinical outcome. *Nat Rev Cancer* 2012;12:298–306.
50 Lin MJ, Svensson-Arvelund J, Lubitz GS, *et al*. Cancer vaccines: the next immunotherapy frontier. *Nat Cancer* 2022;3:911–26.
51 Kirkwood JM, Lee S, Moschos SJ, *et al*. Immunogenicity and Antitumor Effects of Vaccination with Peptide Vaccine +/– Granulocyte-Monocyte Colony-Stimulating Factor and/or IFN-α2b in Advanced Metastatic Melanoma: Eastern Cooperative Oncology Group Phase II Trial E1696. *Clin Cancer Res* 2009;15:1443–51.
52 Melief CJM, Welters MJP, Vergote I, *et al*. Strong vaccine responses during chemotherapy are associated with prolonged cancer survival. *Sci Transl Med* 2020;12:535.
53 Rojas LA, Sethna Z, Soares KC, *et al*. Personalized RNA neoantigen vaccines stimulate T cells in pancreatic cancer. *Nature New Biol* 2023;618:144–50.
54 Borst J, Ahrends T, Bąbała N, *et al*. CD4+ T cell help in cancer immunology and immunotherapy. *Nat Rev Immunol* 2018;18:635–47.
55 Espinosa-Carrasco G, Chiu E, Scrivo A, *et al*. Intratumoral immune triads are required for immunotherapy-mediated elimination of solid tumors. *Cancer Cell* 2024;42:1202–16.
56 Luca BA, Steen CB, Matusiak M, *et al*. Atlas of clinically distinct cell states and ecosystems across human solid tumors. *Cell* 2021;184:5482–96.
57 Welters MJP, Ma W, Santegoets SJAM, *et al*. Intratumoral HPV16-Specific T Cells Constitute a Type I-Oriented Tumor Microenvironment to Improve Survival in HPV16-Driven Oropharyngeal Cancer. *Clin Cancer Res* 2018;24:634–47.
58 Duurland CL, Santegoets SJ, Abdulrahman Z, *et al*. CD161 expression and regulation defines rapidly responding effector CD4+ T cells associated with improved survival in HPV16-associated tumors. *J Immunother Cancer* 2022;10:e003995.
59 Mathy NL, Scheuer W, Lanzendörfer M, *et al*. Interleukin-16 stimulates the expression and production of pro-inflammatory cytokines by human monocytes. *Immunology* 2000;100:63–9.
60 Kaser A, Dunzendorfer S, Offner FA, *et al*. A role for IL-16 in the cross-talk between dendritic cells and T cells. *J Immunol* 1999;163:3232–8.
61 Lynch EA, Heijens CAW, Horst NF, *et al*. Cutting edge: IL-16/CD4 preferentially induces Th1 cell migration: requirement of CCR5. *J Immunol* 2003;171:4965–8.
62 Allen F, Iuliana DB, Rauhe P, *et al*. CCL3 augments tumor rejection and enhances CD8(+) T cell infiltration through NK and CD103(+) dendritic cell recruitment via IFNγ. *Oncoimmunology* 2018;7:e1393598.
63 Galeano Niño JL, Pageon SV, Tay SS, *et al*. Cytotoxic T cells swarm by homotypic chemokine signalling. *Elife* 2020;9:e56554.
64 van Elsas MJ, Middelburg J, Labrie C, *et al*. Immunotherapy-activated T cells recruit and skew late-stage activated M1-like macrophages that are critical for therapeutic efficacy. *Cancer Cell* 2024;42:1032–50.
65 Mami-Chouaib F, Blanc C, Corgnac S, *et al*. Resident memory T cells, critical components in tumor immunology. *J Immunother Cancer* 2018;6:87.
66 Kodelja V, Müller C, Politz O, *et al*. Alternative macrophage activation-associated CC-chemokine-1, a novel structural homologue of macrophage inflammatory protein-1 alpha with a Th2-associated expression pattern. *J Immunol* 1998;160:1411–8.
67 Korbecki J, Olbromski M, Dzięgiel P. CCL18 in the Progression of Cancer. *Int J Mol Sci* 2020;21:7955.
68 Sui X, Chen C, Zhou X, *et al*. Integrative analysis of bulk and single-cell gene expression profiles to identify tumor-associated macrophage-derived CCL18 as a therapeutic target of esophageal squamous cell carcinoma. *J Exp Clin Cancer Res* 2023;42:51.